Proc. of the 2017 IEEE International Conference on Signal and Image Processing Applications (IEEE ICSIPA 2017), Malaysia, September 12-14, 2017

ISAR Imaging using Circularly Polarized Antennas in an Anechoic Chamber

Mohd Zafri bin Baharuddin
Electronics and Communication Engineering Department
College of Engineering, Universiti Tenaga Nasional
Kajang, Selangor, Malaysia

Yuta Izumi, Josaphat Tetuko Sri Sumantyo,
Center for Environmental Remote Sensing
Chiba University
Chiba Japan

Sevket Demirci
Electrical and Electronics Engineering Department
Faculty of Engineering, Mersin University
Yenisehir, Mersin, Turkey

***Abstract*—Synthetic aperture radar (SAR) imaging is typically performed using linearly polarized (LP) signals. There are not many SAR systems utilizing circularly polarized (CP) signals. Recent trends show investigation into CP such as Compact SAR resulting in reduced system size and images with distinct characteristics due to CP signals. To gain insight into a full CP SAR system, we begin study in a controlled environment. This paper presents the design and testing of a wideband inverse synthetic aperture radar (ISAR) system using CP antennas for both receive and transmit. Data measurement setup was constructed in an anechoic chamber with the use of a vector network analyzer (VNA) and automated rotary turntable to revolve targets. We present the measurement procedures for CP imaging, followed by imaging results of canonical targets made using uncalibrated data for CP and compared them with LP ISAR images to illustrate the differences between the two polarizations. This work will lead to the investigation of generating images from CP receive and transmit signals, CP polarimetric decomposition, improvement of related imaging algorithms for CP signals and suitable antenna design.**

Keywords—Anechoic chambers, inverse synthetic aperture radar, network analyzer, radar polarimetry, scattering parameters

I. INTRODUCTION

Mapping of geographical information typically relies on data obtained from ground level soil investigation with multiple in-situ measurements [1]. Earth observation from aerial and spaceborne platforms using synthetic aperture radar (SAR) has provided scientists and researchers with a much faster mode of obtaining the planet's physical surface information, in all weather, day and night [2]. SAR systems can be categorized by their operating frequency bands, bandwidth, and antenna polarization. Typical SAR systems utilize linearly polarized (LP) antennas such as JAXA's ALOS(PALSAR) and ALOS-2(PALSAR-2) [3], the Canadian Space Agency's Radarsat-2 [4], DLR's spaceborne TerraSAR-X satellites [5], NASA's airborne UAVSAR [6], and ONERA's Airborne SAR Imaging Systems [7]. Full polarimetric imaging analysis has been extensively studied for spaceborne and airborne SAR that use linearly polarized measurements. There are not many SAR systems using circular polarization (CP) for imaging targets. Recent trends show some investigation into CP imaging due to its advantages. Compact SAR is a mode that is gaining ground where the system receiver is linearly polarized but the transmitter is circularly polarized. The Japanese Aerospace Agency has an experimental compact SAR mode on their ALOS-2 earth observation satellite [2]. Several SAR systems have begun attempts to use CP antennas for both receive and transmit [8][9]. CP antennas are typically employed in various broadcasting, communication and global positioning applications due to the advantages of insensitivity to antenna orientation, reduced multipath fading effect [10], water particle detection and weather clutter reduction [11]. Rain or hail detection can be increased or decreased according to CP receive-transmit polarization pairs [12][13].

In supporting our goal of a proposed spaceborne circularly polarized synthetic aperture radar (CP-SAR) imaging platform, an unmanned aerial vehicle (UAV) and an initial ground-based test-bed was developed to evaluate outdoor performance of the required RF transceiver, chirp-pulse generator and antenna subsystems [8][14]. Then, to gain insight into a full CP system, we brought the study into a controlled environment. We developed a SAR system for use in an anechoic chamber using a vector network analyzer (VNA) as the signal generator and capturing device to test our antennas as well as imaging algorithms for CP signals [15]. We adopted an inverse synthetic aperture radar (ISAR) configuration where the relative motion of a target with respect to a stationary radar transceiver is utilized to generate an image of the target. The turntable-based ISAR was implemented because it is similar to the spotlight mode in wide angle systems for increased resolution.

Past literature shows lack of real CP data in a controlled environment such as an anechoic chamber [16]–[19]. The systems developed in this work are different from most

This work was supported by the Japanese Ministry of Education, Culture, Sports, Science and Technology (MEXT), and the Japan International Cooperation Agency (JICA).

Proc. of the 2017 IEEE International Conference on Signal and Image Processing Applications (IEEE ICSIPA 2017), Malaysia, September 12-14, 2017

previous work in that this work seeks to use circularly polarized radiation signals to generate images. In experiments, we imaged canonical targets to compare with theoretical scattering responses. This work will lead to the target decomposition investigation of images generated from CP signals, improvement in related imaging algorithms for CP signals and suitable antenna design.

This paper presents the design and measurement procedures of a wideband ISAR system in an anechoic chamber using CP antennas. Section II of this paper will briefly compare the CP and LP theoretical scattering matrix for several canonical targets which sets our experiment expectations. Section III introduces the C-band ISAR measurement system design using circularly polarized antennas. For comparison, measurements were made using both CP and LP antennas for several canonical targets. The results were then processed and presented. Highlights of the results are discussed in section IV and show agreement with scattering theory.

II. Polarimetric Scattering Matrix

A real target presents a complex scattering response due to its complex geometrical structure and reflectivity properties. As an initial study, non-complex canonical targets were used. We used the Sinclair scattering matrix, $\boldsymbol{S}$, to express the polarimetric signature of the targets. Table 1 shows the scattering matrices for flat plate, dihedral and thin vertical pole reflectors, for linear and circular polarizations. Matrices for other canonical targets is documented in [20] and measured LP experiments were proven, however there are few fully polarimetric CP experiments in recent literature. Cartesian polarization basis (H, V) is the LP response where H stands for horizontal polarization and V for vertical. On the other hand, Cartesian polarization basis (L, R) is the CP response where L is for left-handed circularly polarized (LHCP) and R is for right-handed (RHCP).

TABLE I

Linear and Circular Polarization Basis Scattering Matrices

Cartesian polarization basis, $\boldsymbol{S}$	Flat plate reflector	Dihedral reflector	Thin vertical pole
$S_{linear} = \begin{bmatrix} S_{HH} & S_{HV} \\ S_{VH} & S_{VV} \end{bmatrix}$	$\begin{bmatrix} 1 & 0 \\ 0 & 1 \end{bmatrix}$	$\begin{bmatrix} 1 & 0 \\ 0 & -1 \end{bmatrix}$	$\begin{bmatrix} 0 & 0 \\ 0 & 1 \end{bmatrix}$
$S_{circular} = \begin{bmatrix} S_{LL} & S_{LR} \\ S_{RL} & S_{RR} \end{bmatrix}$	$\begin{bmatrix} 0 & j \\ j & 0 \end{bmatrix}$	$\begin{bmatrix} 1 & 0 \\ 0 & -1 \end{bmatrix}$	$\frac{1}{2}\begin{bmatrix} 1 & -j \\ -j & 1 \end{bmatrix}$

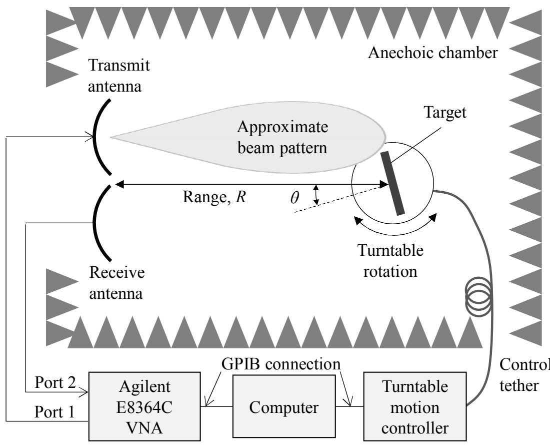

Fig. 1. Measurement geometry and configuration with flat plate target on a turntable assumed for the imaging problem.

For a flat plate reflector, the scattering matrix shows that when imaging using LP antennas, the backscattered signals are still in the same polarization. Thus, using receive-transmit antenna pairs with the same polarization (HH, VV) will provide the strongest reflection response. However, for CP signals a left-handed circularly polarized signal hitting a flat plate will reflect a right-handed circularly polarized signal. As depicted in Table 1, in the case of CP signals, it is expected that using antennas of opposite polarization (LR, RL) will provide the best reflection. The scattering matrices of the three canonical targets were proven through measurements shown in the following section. The flat aluminum plate is 12λ × 18λ in size, the dihedral is 18λ × 9λ for each panel, and the thin poles are 18λ in length.

III. Polarimetric SAR Measurement Setup

Inverse synthetic aperture radar is an imaging mode that takes into account the relative motion of a target with respect to a stationary receiving/transmitting antenna to image that said target. To generate an image of a target from the returned RF signals, two conditions need to be satisfied. First, backscattered data has to be in a two-dimensional format, and second, radar imaging geometry can provide returned data that contains slightly different geometrical information about the target. For the first condition, a frequency varying wave was used to obtain the range resolution. The second condition was met by using a turntable for cross-range measurement.

A. Measurement Geometry and Configuration

Reflection measurement geometry and configuration is shown in Fig. 1. The target to be observed was placed on a polystyrene turntable at a range distance, R, away from the antennas so that the incident wave can be considered as a plane wave. The turntable angle, θ, can be controlled to an angular resolution of 0.1°.

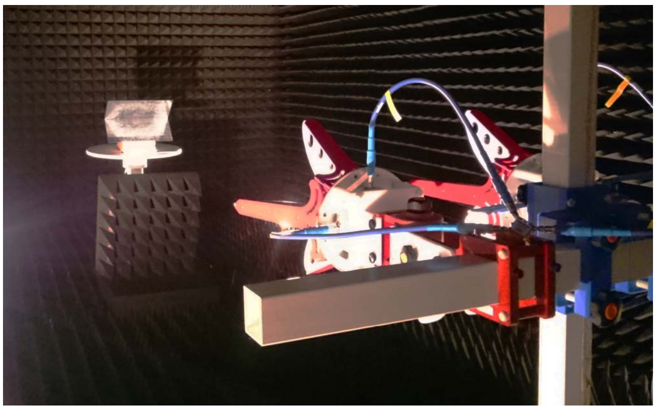

Fig. 2. Horn antennas with phase shifters used for circular polarization (right) and a dihedral reflector for point target measurement placed on a rotating polystyrene platform (far left). Note the quasi-monostatic placement of the receive and transmit antennas.

Antennas were placed in a quasi-monostatic arrangement such that center of the receive and transmit antennas are spatially separated by a distance of 300 mm apart as seen in Fig. 2. A set of open boundary quad-ridged horn antennas with operating capability between 700 MHz to 10 GHz was utilized to generate LP signals [21]. The same antennas were used to generate CP signals with the use of 90° phase shifters. We confirmed the CP setup of each antenna by performing axial ratio measurements in the anechoic chamber. The antennas and target mid-points were all located at the same height, 1.50 meters above the ground level with zero incidence angle.

Setting up the VNA correctly is critical to ensure good response data is captured. Important settings for the VNA are center frequency, frequency span, transmit power, scattering measurement, number of sampling points and time-domain gating. For transmit power, the maximum possible value was set to ensure good signal-to-noise ratio. Transmit power was set to 5 dBm (3.16 mW). A C-band signal was generated with a center frequency of 6.0 GHz and bandwidth of 4.0 GHz using a VNA. The fractional bandwidth is thus 130% which puts our measurement in the ultra-wideband range. To avoid aliasing, the minimum sampling number was chosen to be at least 801 points [15]. A measurement is made at each rotating angle.

B. Single Point CP Range Measurement

A point target measurement was first made to test the validity of the measured data. First the frequency range, number of measurement points, and transmit power are set using values that were discussed in section III-A. Then the VNA was calibrated to these settings with a 2-port calibration at the antenna connection points. Circularly polarized antennas were used for both receive and transmit. This setup of the antennas with the target on the turntable can be seen in Fig. 2.

Frequency response of the chamber without a target was first measured and saved as background noise data, S_{bn}. Measured data consists of complex values of the scattering readings. The target was then placed perpendicular to the radar and the data captured and saved as measured data, S_m. Using (1) we calculated the single range data bin with background noise removed, S_r, in the frequency domain and the CP response for each polarization is as shown in Fig. 3.

$$S_r(f, \theta) = S_m(f, \theta) - S_{bn}(f, \theta) \quad (1)$$

The VNA can be used to quickly confirm the target location by converting the frequency points to backscattering coefficients versus range profile in time domain using Inverse Fast Fourier Transform (IFFT). Since we have set the sampling rate and frequency range, the frequency interval Δf is known. The maximum theoretical range, R_{max}, can then be calculated using (2) to convert the time domain into distance.

$$R_{max} = c / (2\,\Delta f) \quad (2)$$

A time domain gating windowing function was used to obtain data only for the desired target zone. The transformed waveforms showing measured scattering response of the target

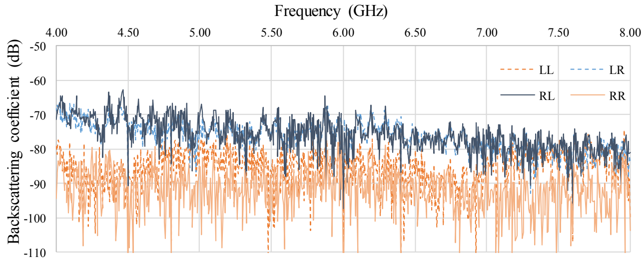

Fig. 3. CP frequency response of a flat plate reflector at C-band 4-8 GHz with background noise removed. Note the relatively high readings for cross-polarized setup compared to co-polarization.

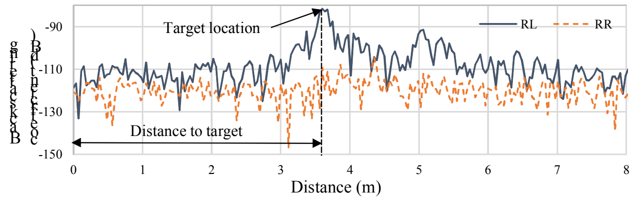

Fig. 4. Range profile of RL and RR data for perpendicular flat plate reflector after IFFT range compression.

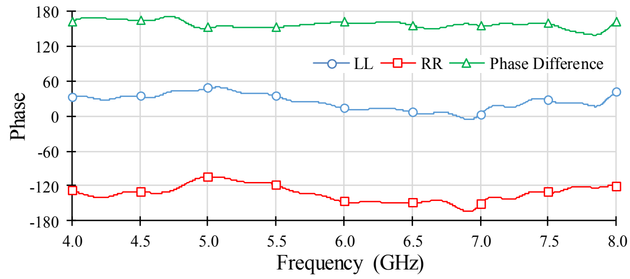

Fig. 5. Phase difference of the co-polarized scattering signals detected from a dihedral reflector is close to 180 degrees.

perpendicular to the antenna illumination are shown in Fig. 4. The detected distance matches the actual location in the setup. The low co-polarized and high cross-polarized amplitude readings in Fig. 4 confirms polarimetric measurement of a flat plate target.

We could also confirm that measured phases was in line with scattering theory. The phase, ϕ, of a target was calculated by taking scattering signals of a perpendicularly placed target and multiplying it by a phase factor:

$$\phi(f,\theta) = e^{j(k_r \cdot R)} \times S_r(f,\theta) \quad (3)$$

where the wave number k_r is $4\pi f/c$ and R is the range distance to the target. Fig. 5 shows uncalibrated phase of CP co-polarized (LL and RR) scattering signals detected from a dihedral. The difference between the two phases is close to the theoretical value of 180° and shows that the system can evaluate phase changes. The phase precision can be further improved with polarimetric calibration.

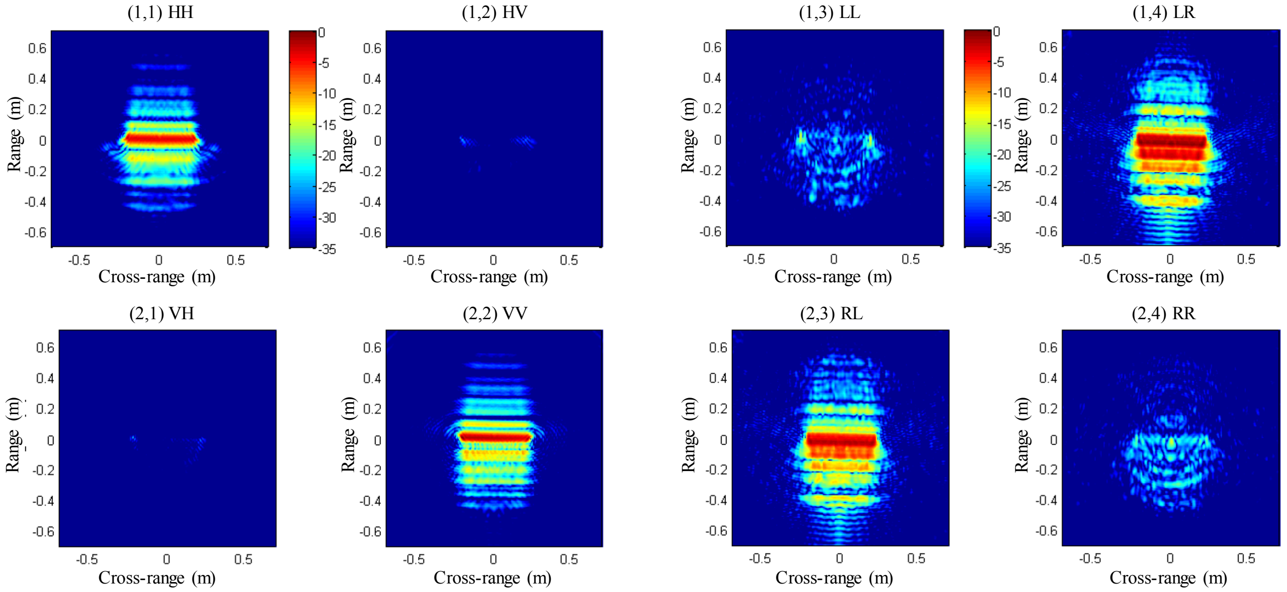

(a) LP imaging output (b) CP imaging output

Fig. 6. Comparison of linear (LP) and circular polarized (CP) imaging output of a canonical flat plate reflector.

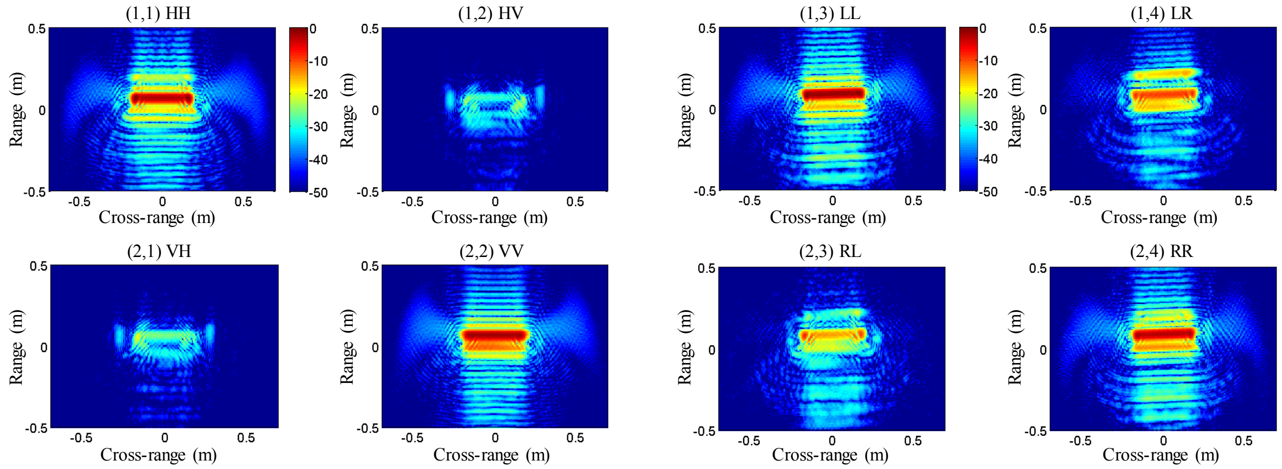

(a) LP imaging output (b) CP imaging output

Fig. 7. Comparison of linear (LP) and circular polarized (CP) imaging output of a dihedral reflector.

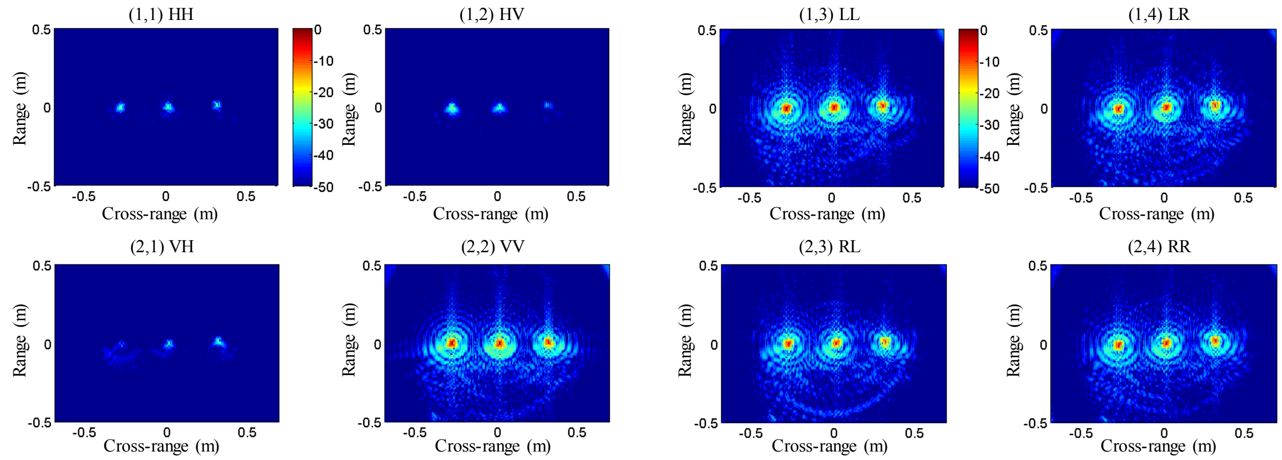

(a) LP imaging output (b) CP imaging output

Fig. 8. Comparison of linear (LP) and circular polarized (CP) imaging output of three thin vertical poles.

Fig. 9. Model turboprop airplane made of balsa wood as a complex target.

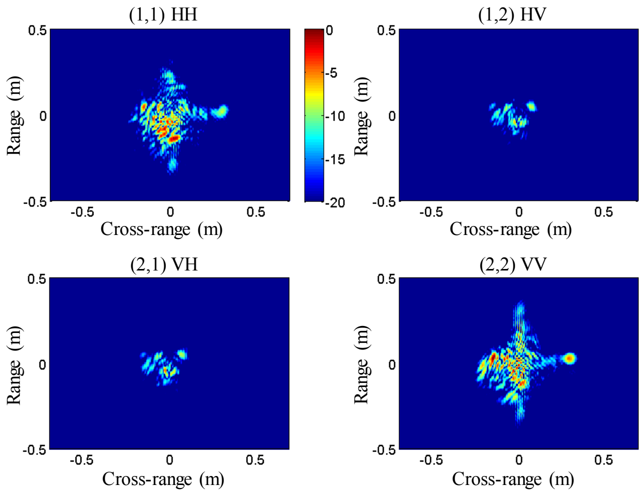

(a) LP imaging output

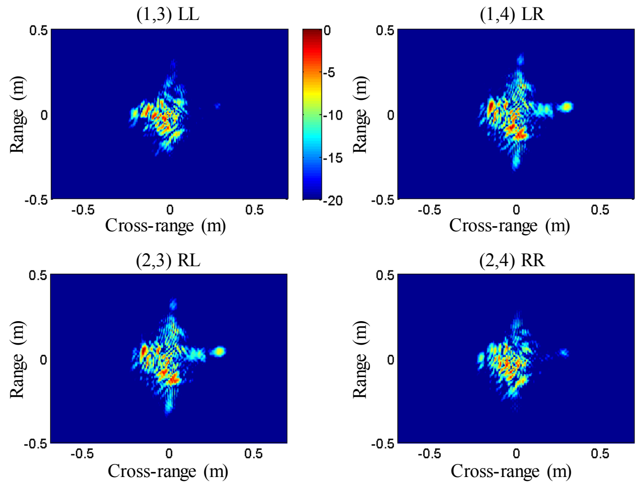

(b) CP imaging output

Fig. 10. Resulting images of the developed system on a complex target.

C. ISAR Measurement

The next step towards imaging the target is to collect scattering responses at multiple angles. The turntable angle θ was rotated from 0° to 180° with a resolution, $\Delta\theta$, of 1.0° for a total of 180 points. At each angle, the turntable stops and makes a measurement with the same VNA settings as previously explained. A customized computer program which communicates via a general-purpose interface bus (GPIB) controls the turntable rotation angle, measurement trigger and data logging. Finally, to obtain an image of the scene using the measured range bins, cross-range compression needs to be performed. This was done with a back-projection algorithm [22][23]. The process above was repeated for all CP and LP polarimetric combinations by changing the horn antenna configuration. The generated images for a rectangular plate reflector for LP and CP are shown in Fig. 6 for comparison.

Fig. 6(a) shows LP imaging results. The images are normalized and displayed with a wide dynamic range to understand the scattering effects. We can remove the ripples around the target by simply limiting the dynamic range to around -20 dB. As can be seen in image (1,1) and (2,2) of Fig. 6 (a), the aluminum plate can be visualized when using co-polarized configurations. Images (1,2) and (2,1) show that cross-polarized LP antennas can still barely detect the target since there are fringing effects at the sides of the target.

Fig. 6(b) shows imaging results when using CP antennas. The cross-polarized results in image (1,4) and (2,3) are as expected from a flat plate target and consistent with the respective theoretical scattering matrix. Some scattering was detected at the target location, which may be due to edge reflections or antenna cross-polarization impurity. The polystyrene column used for mounting was not detected in any measurement. Observation of the full polarimetric imaging results for both CP and LP are consistent with theoretical polarimetric scattering response of a flat plate.

We next tested a dihedral reflector and again confirmed that the measured scattering matches with the theory in literature. The reconstructed dihedral images are shown in Fig. 7. Phase information was also retained as explained in Section III-B. Finally, imaging of three identical thin vertical poles spaced 450mm apart is shown in Fig. 8. The metal poles have a diameter of 2 mm. We selected the diameter of the poles to be much smaller than the smallest wavelength to ensure sensitivity to reflector orientation. LP images of the vertically oriented poles are as expected showing good scattering for VV and no scattering for all other polarization pairs. The individual poles can be clearly imaged with matching scattering responses. CP images, on the other hand, have scattering for all receive-transmit pairs. Together with the phase information, these are the results that we consider valuable for continuing polarimetric SAR studies.

Finally, a model turboprop airplane 35 cm in length and with a 40 cm wingspan entirely made of balsa wood was used as a complex target, as shown in Fig. 9. It mostly has flat surfaces on the sides with many curvatures on the front, tail and wings. Both LP and CP measurements were made resulting in images of Fig 10. We can make out the shape and orientation of the airplane based on the resulting images. In some images such as in (2,2) and (1,4) the tail provided a strong reflection. The center of each image is quite cluttered due to scattering from the propellers and landing wheels. However, as predicted, cross-polarized LP could not image the target. CP measurements had images in all receive-transmit pairs. These results on a complex target are consistent with output from the canonical targets.

IV. Conclusion

In this paper we introduced a system in an anechoic chamber to study fundamentals and test variation in circularly polarized ISAR imaging solutions. Measurement procedures were presented in detail and captured data was imaged using a back-projection algorithm. Imaging output of canonical targets are consistent with theoretical scattering responses for both CP and LP in magnitude and phase. From now, non-canonical targets can be imaged and provide a point to continue the study of polarimetric decomposition. The system is a step towards developing a spaceborne CP SAR system in our laboratory. Further work will include testing the scattering response of more complex targets and improving polarimetric calibration for a calibrated CP image.

References

[1] N. Z. Baharuddin, R. C. Omar, R. Roslan, N. H. N. Khalid and M. I. M. Hanifah, "Determination Of Slope Instability Using Spatially Integrated Mapping Framework," 2016 IOP Conf. Ser.: Mater. Sci. Eng., vol. 160, no. 1, December 7, 2016.

[2] A. Moreira, P. Prats-Iraola, M. Younis, G. Krieger, I. Hajnsek and K. P. Papathanassiou, "A tutorial on synthetic aperture radar," in IEEE Geoscience and Remote Sensing Magazine, vol. 1, no. 1, pp. 6-43, March 2013.

[3] Y. Kankaku, Y. Osawa, S. Suzuki, and T. Watanabe, "The overview of the L-band SAR onboard ALOS-2," Proc. PIERS, Moscow, 2009, pp.735-738.

[4] P. A. Fox and C. Grenier, "The RADARSAT-2 synthetic aperture radar antenna phased array error analysis and performance," Phased Array Systems and Technology, 2003. IEEE Int'l Symp. on, 2003, pp. 247-252.

[5] S. Buckreuss, U. Steinbrecher and B. Schättler, "The TerraSAR-X mission status," IEEE 5th Asia-Pacific Conference on Synthetic Aperture Radar (APSAR), Singapore, 2015, pp. 357-361.

[6] Y. Lou, S. Hensley, R. Chao, E. Chapin, B. Heavy, C. Jones, T. Miller, C. Naftel, and D. Fratello, "UAVSAR instrument: current operations and planned upgrades," Earth Science Technology Forum, Pasadena, CA: Jet Propulsion Laboratory, National Aeronautics and Space Administration, June 21, 2011.

[7] J. F. Nouvel, X. Dupuis and M. Lesturgie, "Non line of sight signal analysis: Investigation of interferometry modes over urban area," IEEE 5th Asia-Pacific Conference on Synthetic Aperture Radar (APSAR), Singapore, 2015, pp. 582-586.

[8] J.T. Sri Sumantyo, "Circularly polarized synthetic aperture radar onboard unmanned aerial vehicle (CP-SAR UAV)," Autonomous Control Systems and Vehicles, Intelligent Systems, Control and Automation: Science and Engr., Vol. 65, Springer, 2013, pp. 175-192.

[9] C. N. Koyama and M. Sato, "Detection and classification of subsurface objects by polarimetric radar imaging," 2015 IEEE Radar Conference, Johannesburg, 2015, pp. 440-445.

[10] F. Yildirim, A. S. Sadri and H. Liu, "Polarization effects for indoor wireless communications at 60 GHz," in IEEE Communications Letters, vol. 12, no. 9, September 2008, pp. 660-662.

[11] P. A. Lynn, "Signal processing and display," in Radar Systems, Springer, 1987, pp. 76.

[12] K. J. Al-Jumily, R. B. Charlton, and R. G. Humphries, "Identification of Rain and Hail with Circular Polarization Radar," in J. Appl. Meteor., 30, 1991, pp. 1075–1087.

[13] S. Okamura, and T. Oguchi, "Electromagnetic Wave Propagation in Rain and Polarization Effects," Proc. Japan Academy, Series B, Physical and Biological Sciences 86.6: 2010, pp. 539–562.

[14] M. Z. Baharuddin, K. Suto, J. T. S. Sumantyo, H. Kuze, L. T. Sze, J. Y. K. Shen, W. G. Cheaw, K. V. Chet, "Development of a semi-automated SAR test-bed," IEEE 2nd Intl. Symp. on Telecommunication Technologies (ISTT), Langkawi, 2014, pp. 236-240.

[15] M. Z. Baharuddin, B. Setiadi, J.T.S. Sumantyo, H. Kuze, "An experimental network analyzer based ISAR system for studying SAR fundamentals," in IEEE 5th Asia-Pacific Conference on Synthetic Aperture Radar (APSAR), Singapore, 1-4 Sept. 2015, pp.103-107.

[16] C.C. Chen, H.C. Andrews, "Target-motion-induced radar imaging," IEEE Tran. Aerospace Electronic Systems, Vol. AES-16, No. 1, 1980, pp. 2-14.

[17] Y. Bennani, F. Comblet, A. Khenchaf, "RCS of complex targets: original representation validated by measurements—application to ISAR imagery," IEEE Trans. on Geoscience and Remote Sensing, Vol. 50, No. 10, 2012, pp. 3882-3891.

[18] J. W. Bredow, R. L. Porco and G. Hartman, "Circular and Linear Polarization Inverse Sar Imaging of Simple Deterministic Targets and Statistically Known Randomly Rough Surfaces Using Constant and Varying Illumination," Geoscience and Remote Sensing Symp., 1992. IGARSS '92. International, Houston, TX, USA, 1992, pp. 1193-1194.

[19] S. Okamura, K. Takahashi and M. Sato, "Non-destructive inspection of buildings using radar polarimetry," Synthetic Aperture Radar (APSAR), 2013 Asia-Pacific Conference on, Tsukuba, 2013, pp. 122-125.

[20] J.S. Lee, E. Pottier, Polarimetric Radar Imaging from basics to applications, CRC Press, 2009, pp. 92-98.

[21] ETS Lindgren, Wireless Antennas: Open Boundary Quad-Ridged Horn, technical specifications datasheet, revision A, 2007.

[22] S. Demirci, H. Cetinkaya, E. Yigit, C. Ozdemir and A. Vertiy, "A study on millimeter-wave imaging of concealed objects: application using back projection algorithm," PIER, vol. 128, 2012, pp. 457-477.

[23] M. Soumekh, "Spotlight synthetic aperture radar," in Synthetic Aperture Radar Signal Processing with MATLAB Algorithms, 1st ed. Wiley-Interscience, New York, 1999.